Guided and defect modes in periodic dielectric waveguides

Shanhui Fan, Joshua N. Winn, Adrian Devenyi, J. C. Chen, Robert D. Meade, and J. D. Joannopoulos

Department of Physics and Research Laboratory of Electronics, Massachusetts Institute of Technology, 77 Massachusetts Avenue, Cambridge, Massachusetts 02139

Received June 9, 1994; revised manuscript received November 23, 1994

The nature of guided modes and defect modes in periodic dielectric waveguides is investigated computationally for model systems in two dimensions. It is shown that defect states that exist within the band gap of guided modes can be excited to form tightly localized high-Q resonances.

1. INTRODUCTION

Periodic dielectric materials offer a great deal of control over the propagation of light.[1] Usually the basic idea is to design periodic dielectric structures that have a band gap for a particular frequency range. In a recent study[2] Meade *et al.* showed that defects in a three-dimensional (3-D) periodic dielectric material (photonic crystal) can admit localized states within a band gap. It is the purpose of this paper to investigate the characteristics and properties of modes in periodic dielectric waveguides. In particular, we are interested in understanding the nature of guided modes and whether defects can lead to highly localized resonances.

Before we present our model systems it is useful to consider guided modes in a uniform dielectric waveguide. A schematic rectangular waveguide is shown in Fig. 1(a). Because of the translational symmetry along the slab the mode can be characterized by wave vector $k_\parallel$. The dispersion relation $\omega(k_\parallel)$ is also sketched in Fig. 1(a). Modes above the light line ($\omega = k_\parallel$) are radiating modes, with a continuous spectrum. Below the light line are guided modes, which have a discrete band structure. The guided modes that make up a given band have the same symmetry and similar polarization properties.

We can consider a small periodic index contrast along the waveguide to be a weak perturbation of a uniform slab. (A typical example is the corrugated grating on the surface of a thin-film waveguide in a distributed-feedback laser.) For such a system a unit cell of length a is repeated along the waveguide, and modes can be characterized by a wave vector $k_\parallel$ that is confined to the first Brillouin zone. The perturbation-induced coupling between the modes at $k_\parallel = \pi/a$ and $k_\parallel = -\pi/a$ opens up small gaps at the zone edge [see Fig. 1(b)]. Light cannot propagate along the waveguide with a frequency within the gap since there are no permitted propagating states. This phenomenon can also be readily understood by Bragg's condition—multiple reflections from the different unit cells conspire to interfere destructively within the structure.

In distributed-feedback laser systems the translational symmetry is broken by placement of a phase shift into the structure. The phase shift can be designed (for example, by use of a $\lambda/4$ phase shift) so that a weakly localized mode is created inside the gap.[3] This mode would act as the lasing mode. However, since the band gap is small the localized mode will decay gradually into the periodic system. For a frequency difference $\delta\omega$ between the bottom of the upper band and the defect mode, the decay length is roughly proportional to $\delta\omega^{-0.5}$. The introduction of a small index contrast and phase shift in distributed-feedback lasers results in a narrow linewidth and single-longitudinal-mode operation.[3] Increasing the index contrast, we expect a larger gap to emerge, as in Fig. 1(c), which might permit us to create a high-Q defect resonance inside the gap. The purpose of this study is to explore this possibility.

The format of the paper is as follows: In Section 2 we begin with a description of our model systems and the techniques used for the calculations. In Section 3 the results of our calculations on several model systems are presented, with emphasis on identifying defects that give rise to strongly localized resonances for different polarizations. Finally, in Section 4 we conclude with a summary of our results and discussions of future directions.

2. CALCULATIONAL DETAILS

A. Model Systems

We chose to perform studies on two-dimensional (2-D) model systems, with the hope of eliciting all the essential physical properties. By 2-D we mean systems in which there is no variation in the fields or dielectric constant in the z direction and waves propagate only in the x–y plane. In these 2-D systems any mirror-reflection operator about the z axis leaves the system invariant and permits all the modes to decouple rigorously into two symmetry classes. One class of modes can be classified as transverse electric (TE), in which the magnetic field points in the z direction and the electric field lies in the x–y plane, and the other class is transverse magnetic (TM), in which the electric field points in the z direction and the magnetic field lies in the x–y plane.[4] Maxwell's equations are decoupled for these two polarizations, so we can investigate the properties of each independently. 2-D systems are more amenable to computation than their 3-D counterparts, and their fields are much easier to visualize. In a 3-D periodic waveguide, modes may still be roughly characterized as TE-like or TM-like according to their dominant polarization directions. We hope that the knowledge

0740-3224/95/071267-06$06.00

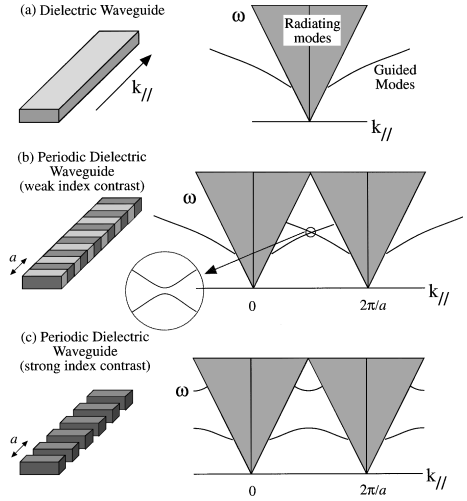

Fig. 1. Schematic of the band structures for waveguides with different dielectric-constant contrast along the guide. (a) Uniform dielectric waveguide, with the band structure shown on the right-hand side. (b) Periodic dielectric waveguide with weak index contrast. The origin of the gap is shown on the right-hand side. (c) Periodic dielectric waveguide with strong index contrast. The expected band structure is sketched on the right-hand side.

gained from 2-D models can be readily applied to more realistic 3-D systems.

Finally, we note that TM (TE) modes, defined as above in terms of the 2-D plane normal, correspond, respectively, to the conventional TE (TM) modes defined with respect to the propagation direction along a traditional waveguide. We adopt the former definition throughout this paper because of its wider applicability to 2-D mixed dielectric medias in general (e.g., for localized states with no identifiable propagation direction).

B. Methods of Computation

In general, the detailed characteristics of light propagation and confinement cannot be determined analytically for complex dielectric structures. Accurate numerical methods are available for this purpose. We applied two complementary schemes to deal with different aspects of these systems. A frequency-domain approach was used to find the eigenmodes of perfect systems and systems with defects. A time-domain approach was then applied to study the transient properties and the quality factor Q of the localized defect modes.

1. Frequency-Domain Approach

We can obtain a single governing equation for electromagnetic modes by rearranging Maxwell's equations ($c = 1$):

$$\nabla \times \left[\frac{1}{\varepsilon(\mathbf{r})} \nabla \times \mathbf{H} \right] = \omega^2 \mathbf{H}. \tag{1}$$

Here $\varepsilon(\mathbf{r})$ is the dielectric function and $\mathbf{H}$ is the magnetic field of an electromagnetic mode of frequency ω. If $\varepsilon(\mathbf{r})$ is periodic, the magnetic field, which must be transverse, is expanded in a basis of transverse plane waves $\mathbf{e}_\lambda \exp[i(\mathbf{k} + \mathbf{G}) \cdot \mathbf{r}]$, where $\mathbf{k}$ is in the first Brillouin zone, $\mathbf{G}$ is a reciprocal lattice vector, and $\mathbf{e}_\lambda$ are the unit vectors perpendicular to wave vector $\mathbf{k} + \mathbf{G}$. In this basis Eq. (1) becomes a matrix eigenvalue equation:

$$\sum_{(\mathbf{G}\lambda)'} \Theta^{\mathbf{k}}_{(\mathbf{G}\lambda),(\mathbf{G}\lambda)'} h_{(\mathbf{G}\lambda)'} = \omega^2 h_{(\mathbf{G}\lambda)'}, \tag{2}$$

where $h_{\mathbf{G}\lambda}$ is the coefficient of the plane wave $\mathbf{e}_\lambda \exp[i(\mathbf{k} + \mathbf{G}) \cdot \mathbf{r}]$. The matrix is defined by

$$\Theta^{\mathbf{k}}_{(\mathbf{G}\lambda),(\mathbf{G}\lambda)'} = [(\mathbf{k} + \mathbf{G}) \times \mathbf{e}_\lambda] \cdot [(k + \mathbf{G}') \times \mathbf{e}_{\lambda'}] \varepsilon^{-1}(\mathbf{G}, \mathbf{G}'). \tag{3}$$

In this expression $\varepsilon^{-1}(\mathbf{G}, \mathbf{G}')$ is the inverse of the Fourier transform of the dielectric function $\varepsilon(\mathbf{r})$. Standard numerical methods can then be applied to diagonalize the matrix and obtain eigenvalues and eigenmodes. The details are discussed elsewhere.[5]

To model finite dielectric structures, we use the supercell approximation. In this method one embeds the structural geometry of interest in a large supercell that is then repeated periodically in position space. For a perfect periodic dielectric waveguide, one supercell simply contains one period. For a waveguide with a defect, one supercell contains the defect in question and several (typically seven in this study) periods of the waveguide on either side of it. Since the modes of interest will decay exponentially away from the waveguides or cavities, the size of the supercell is chosen large enough so that the coupling between different cells is negligible, and the results can be considered accurate descriptions of a single waveguide or cavity.

2. Time-Domain Approach

To study the time evolution of electromagnetic fields, we applied a finite-difference time-domain scheme to solve the Maxwell equations. For illustrative purposes we present the simplest case, i.e., the wave equation for TM modes in 2-D systems. The case of TE modes is similar, except that the wave equation is slightly modified. Recall that for TM modes the electric field points strictly in the z direction. This single component of the electric field obeys the simple wave equation

$$\frac{\partial^2 E(x, y)}{\partial x^2} + \frac{\partial^2 E(x, y)}{\partial y^2} = \varepsilon(x, y) \frac{\partial^2 E(x, y)}{\partial t^2}. \tag{4}$$

This equation is discretized on a simple square lattice. Space–time points are separated by fixed basic units of time Δt and distance Δs. We can label the time index as n and the space indices as i and j, so that the correspondence $E(i\Delta s, j\Delta s, n\Delta t) \rightarrow \mathbf{E}^n_{ij}$ holds. The dielectric function can be discretized in the same manner: $\varepsilon(i\Delta s, j\Delta s) \rightarrow \varepsilon_{ij}$. We then approximate the derivatives at each lattice point by a corresponding centered difference, giving rise to the finite-difference equation

$$\frac{E^n_{i+1,j} - 2E^n_{ij} + E^n_{i-1,j}}{(\Delta s)^2} + \frac{E^n_{i,j+1} - 2E^n_{ij} + E^n_{i,j-1}}{(\Delta s)^2} = (\varepsilon_{ij}) \frac{E^{n+1}_{ij} - 2E^n_{ij} + E^{n-1}_{ij}}{(\Delta t)^2}. \tag{5}$$

The idea is to solve this relation for the future time component E^{n+1}_{ij} and use this to update the values of the field in the interior of the grid. On the boundary, where information about neighboring points is not available, we applied the second-order transparent boundary condition.

A detailed discussion of this boundary condition as well as other features on finite-difference time-domain simulations can be found in Refs. 6–8.

C. Calculation of Q Value

The quality factor Q of a resonator is defined universally as[9]

$$Q = \frac{\omega E}{P} = -\frac{\omega E}{\mathrm{d}E/\mathrm{d}t}, \tag{6}$$

where E is the stored energy, ω is the resonant frequency, and $P = -\mathrm{d}E/\mathrm{d}t$ is the power dissipated. An equivalent and more descriptive statement is that a resonator can sustain Q oscillations before the energy dies down to $e^{-2\pi} \approx 0.2\%$ of its original values. By excitation of the resonance mode and computation of the energy inside the cell over time with the time-domain scheme it is a straightforward matter to compute Q and quantify the dissipation.

3. RESULTS

Previous studies of photonic crystals have shown that, for a structure with dielectric contrast as high as 13:1, considerations like Bragg's condition (which does not take into account the vector nature of electromagnetic fields) are not sufficient to describe essential physical properties. Waves with different polarizations have different behaviors in most dielectric configurations. Studies of 2-D photonic crystals show that isolated high-dielectric spots are important in developing a photonic band gap for TM-polarized modes, whereas connectivity of high-dielectric material is important for TE band gaps.[10] With that in mind we chose to study two different types of waveguide: a one-dimensional array of dielectric rods and a one-dimensional array of air holes in a dielectric strip. The former structure should give rise to large gap in TM modes, while the latter should be favorable for a large TE gap.

A. Dielectric-Rod Array Waveguide

This structure consists of a single row of dielectric columns in air and is sketched in the inset of Fig. 2(a). The columns have the dielectric constant $\varepsilon = 13$ and generally have a rectangular shape. The spacing between columns defines the lattice constant a. The dimensions of the columns are chosen to be $0.3a \times 0.3a$.

Because the system is periodic along one direction (say, the x axis) we can catalog the eigenmodes according to $\omega(k_x)$, which is done in Fig. 2. States above the light line ($\omega = k_x$) can satisfy the dispersion relation of free space $\omega = |k|$, so these modes are extended in the air regions. On the other hand, states below the light line must be evanescent in the y direction and are guided by the dielectric. Note that for TM modes there is a large range of frequencies in which there are no guided modes [Fig. 2(a)]. We refer to this as a gap, even though it does not extend over the entire Brillouin zone. We chose the structural parameters so that a big gap exists between the first and second TM guided-mode bands. TE bands, as expected, have only a small gap for this structure [Fig. 2(b)].

To gain insight into the nature of gaps here, we examined the field patterns of different modes. The electric field of modes at $k = G/2$ of the first two TM bands are shown in Fig. 3 ($G = 2\pi/a$ is the reciprocal lattice vector). Since both modes are at zone edge the fields alternate in sign from cell to neighboring cell. In Fig. 3(a) we see that the fields associated with the dielectric material are strongly concentrated in the dielectric regions. This contrasts strongly with Fig. 3(b), which shows the field of the second band. Here a nodal plane cuts through all the dielectric rods, and the antinodes occur in the air region between the dielectrics.

The frequency of light for a given wavelength is lower in dielectric material than in air. It seems reasonable,

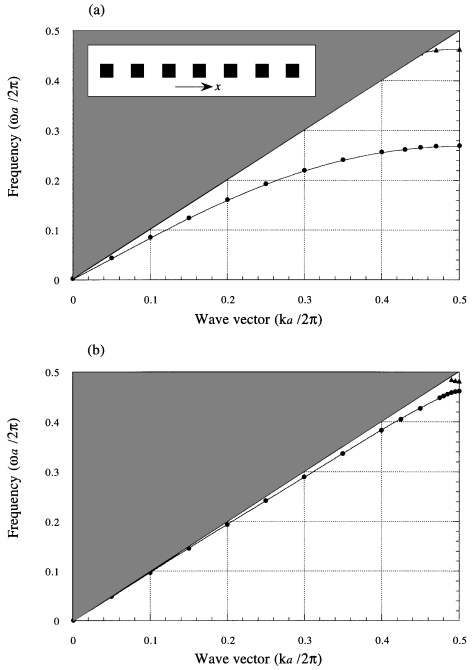

Fig. 2. Calculated band diagrams for the (a) TM and the (b) TE modes in a perfect dielectric-rod waveguide structure. The shaded regions represent extended modes, and the solid curves below the light line are guided modes.

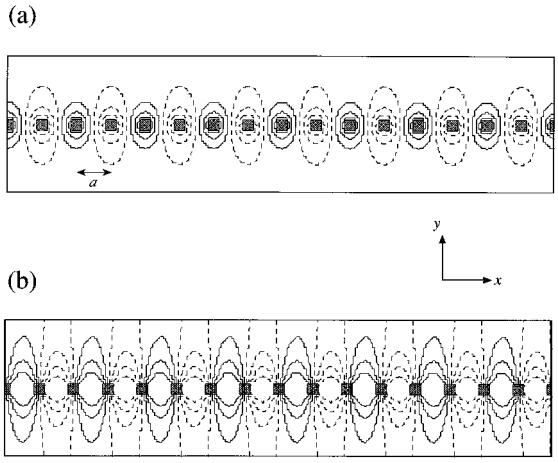

Fig. 3. Contour plots of the TM displacement fields at the zone edge for the (a) first and the (b) second bands in the perfect dielectric-rod waveguide structure. The TM modes have **D** normal to the plane. The dashed curves represent contours with $D_z < 0$, while the solid curves represent contours with $D_z > 0$. The positions of the rods are shown by the shaded areas.

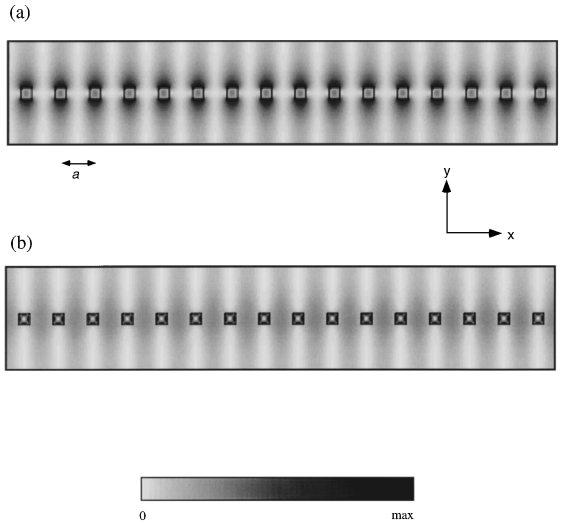

Fig. 4. Gray-scale plots of the power in the electrical fields of TE states at the zone edge for the (a) first and the (b) second bands in the perfect dielectric-rod structure.

then, that eigenmodes that have most of their character in the dielectric region have lower frequency than those with most of their energy in air. This simple observation explains the large splitting between these two bands: the first band has most of its character in the dielectric regions and has a lower frequency, while the second has most of its character in the air and has a higher frequency. In both bands the fields are concentrated along the waveguide and decay exponentially away from it, which is the characteristic of their guided-mode nature.

For TE bands the electric power for the first two modes at the zone edge is shown in Fig. 4. Like the TM modes the TE modes tend to concentrate inside the dielectric regions to lower their frequency. However, there is no continuous pathway between the dielectric rods. Since the field lines must be continuous they must penetrate the air regions. For this reason neither band is strongly concentrated in the dielectric. Since the bands do not contrast strongly with each other they do not have a large frequency splitting. The vector nature of the electromagnetic fields is crucial in explaining this behavior. Also, because both modes have most of their power concentrated in the air region, they are close to the light line, as shown in Fig. 2(b).

One fact worth pointing out is that, for waveguides with spatial period a, modes with frequencies above π/a, in general, are extended modes. As usual, modes are guided if $\omega < k_{\|}$ and extended if $\omega > k_{\|}$. For periodic dielectric waveguides, $k_{\|}$ is constrained in the region $(-\pi/a, \pi/a)$. Modes with frequency $\omega > \pi/a$ will automatically satisfy the extend-mode condition. Thus spatial periodicity imposes an upper-frequency cutoff for guided modes. However, in the continuum of modes with frequency above π/a, we expect that strongly guided resonances can still exist.

To create a localized resonance, we increased the width of a single dielectric rod, as shown in the bottom of Fig. 5. As the width of the dielectric increases, the frequency of the resonance moves through the band gap. The most localized TM mode, with frequency $\omega = 0.3130$, was found for a defect formed by a central column of width $0.8a$. Figure 5 also shows a surface plot of the z component of the displacement field across the supercell. The supercell is composed of seven dielectric columns on each side of the defect. The striking feature of this diagram is the rapid decay of the field amplitude in both the x and y directions. This corresponds to a very low loss of power out of the cavity mode and therefore to a small coupling between nearest-neighbor cavities. All TE resonances for this defect are found to be delocalized.

The quality factor of this resonator was calculated by use of the time-domain method mentioned above. We initialize the system with a certain electric-field configuration and let it evolve according to Eq. (5). For effective excitation of the localized resonance the initial condition should have a large overlap with the defect mode. The energy inside the cell was measured over time and is shown in Fig. 6. For the first few cycles all modes except the high-Q mode radiate away. The defect mode continues its slow exponential decay. The Q value of this mode, calculated from the slope of the logarithmic plot, is $\sim$12,000.

Unlike structures with a complete frequency gap, in which any defect state in the gap must be localized,[2] there

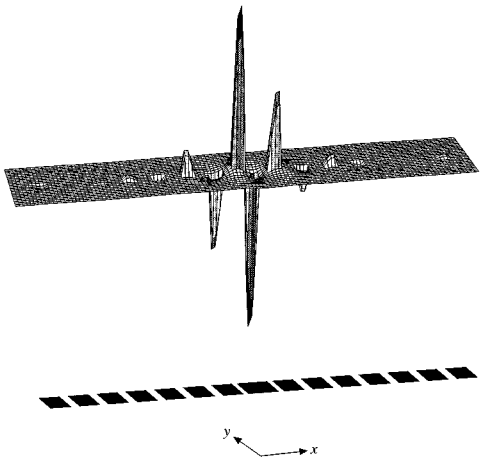

Fig. 5. Plot of the displacement field of the high-Q TM defect mode. The largest positive and negative peaks of the displacement field lie within the dielectric region of the defect. The other peaks of the displacement field lie within the square dielectric elements of the waveguide.

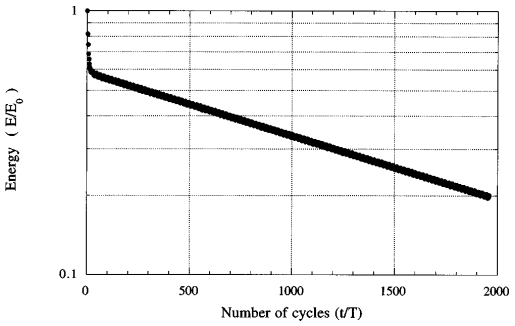

Fig. 6. Transient decay of the high-Q TM defect mode. Plotted is the total energy in the defect mode as a function of time. E_0 is the initial energy in the fields. T is the period of the high-Q defect mode. Since the mode is not excited completely purely the low-Q modes radiate away before the high-Q exponential decay becomes manifest. The Q value for this defect mode is 12,000.

is no complete gap in this structure to ensure localization. It is perhaps surprising to achieve strong localization in the absence of a complete band gap. A simple explanation is that waveguides will support guided modes, but a periodic index contrast will reflect guided modes within a certain frequency range. If the cavity has the proper size to support a mode in the band gap, a localized mode is obtained.

We can understand the results in terms of mode coupling. The addition of dielectric lowers the frequency of a guided mode from the upper band into the gap. This defect mode is primarily a superposition of guided modes from the first two bands. As a result, there is no nodal plane parallel to the waveguide, as can be seen in Fig. 5. However, there will be some coupling between the resonance and the extended states. In the supercell approximation a defect system is approximated by a periodic system with large periodicity L. An exact description is reproduced in the limit that L goes to infinity. From the discussion of cutoff frequency in the periodic dielectric waveguide we know that the upper cutoff is inversely proportional to L, so it goes to zero as the spatial period goes to infinity. Hence, in general, a truly localized state does not exist in such defect systems. Coupling between the resonance and the continuum gives rise to a lateral outflow of energy from the resonance mode. The finite size of the lattice leads to an outflow of energy along the waveguide. These factors cause the resonance to have a finite lifetime, characterized by Q.

Another fact worth noticing is that the frequency of the most strongly localized TM mode is $\omega = a/\lambda = 0.3130$, which is near the bottom of the gap in the periodic structure $\omega = 0.2754$. We generally expect that highest-Q modes will occur at frequencies near the center of the gap, where the decay length is smallest. In one-dimensional cavities a high-Q resonance requires a strong spatial localization, requiring the frequency to be close to the center of the gap. However, it also requires that the mode be localized in k space, so that the overlap between the resonance and the free-space modes is minimized. This requirement can be better satisfied if the resonance frequency is lower. This helps to explain why a high-Q resonance was found in the lower half of the gap.

B. Air-Hole-Array Strip Waveguide

As mentioned above, we expect a connected dielectric structure to be favorable for the existence of TE band gaps. Therefore we chose to study TE modes in the structure shown in the inset of Fig. 7. This is an array of infinite-length air columns ($\varepsilon = 1$) inside a strip of dielectric ($\varepsilon = 13$). The distance between nearest-neighbor air holes defines length unit a. The width of the slab is $1.2a$, and the radius of the holes is $0.36a$. These parameters were optimized to achieve the strongest localization by a defect in this structure. The band structure is shown in Fig. 7. Note that there is a large gap between the first and second guided-mode bands.

Plots of electric power for two band-edge modes are shown in Fig. 8. The TE modes in this system are confined primarily inside the waveguide. Modes in the first band have a displacement field contained in the dielectric surrounding each air hole. However, the second band has much of its power distributed inside the air holes. This difference explains the large frequency difference between these two modes.

We create a defect in the system by increasing the distance d between the two central air holes, as shown in the bottom of Fig. 9. A supercell with seven air holes on either side of the defect was used. We found the most

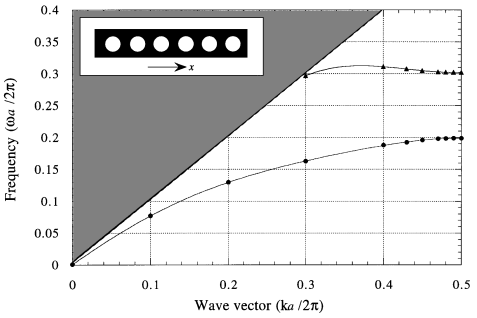

Fig. 7. Calculated band diagram for TE modes in a perfect air-column structure. The shaded region represents extended modes, and the solid curves below the light line are guided modes.

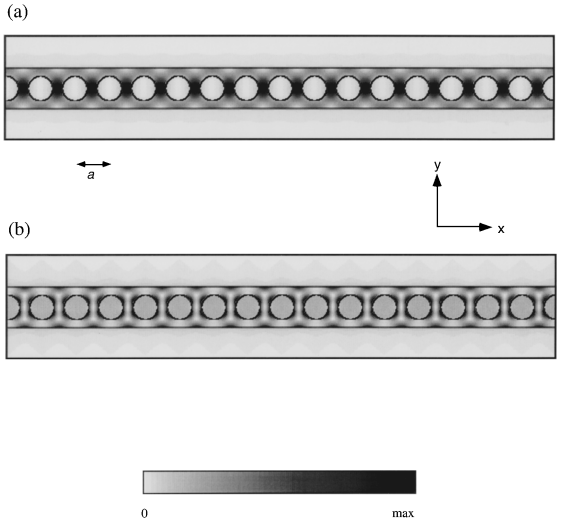

Fig. 8. Gray-scale plots of the power in the electrical fields of TE states at the zone edge for (a) the first and (b) the second bands in the air-column structure.

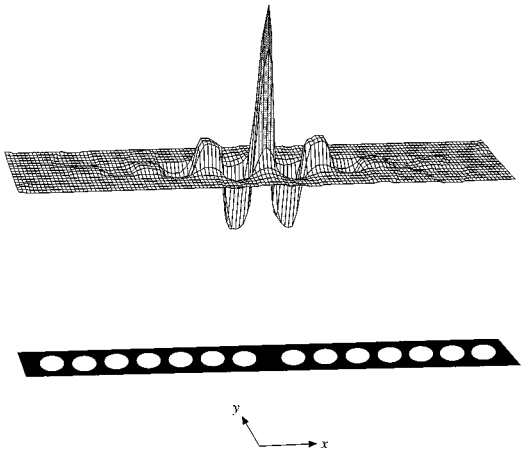

Fig. 9. Plot of the magnetic field of the high-Q TE defect mode. The largest peak in the magnetic field lies within the dielectric region of the defect. The other peaks lie within the circular air regions of the waveguide.

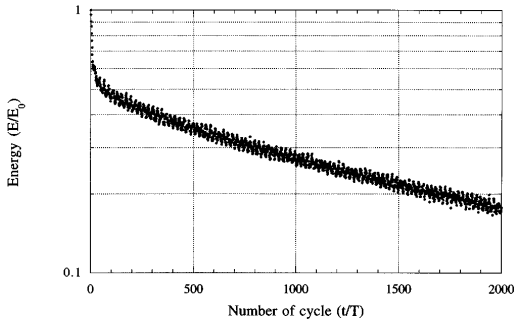

Fig. 10. Transient decay of the high-Q TE defect mode. Plotted is the total energy in the defect mode as a function of time. E_0 and T are in the same convention as in Fig. 6. The Q value of this mode is 13,000.

strongly localized state at $\omega = a/\lambda = 0.2416$ by choosing $d = 1.4a$. Figure 9 also shows the surface plot of the z component of the magnetic field across the supercell. The field amplitude decays rapidly in both the x and y directions.

The time-domain method was supplied to calculate the Q value for this defect mode. The energy inside the cell was measured and is shown on a logarithmic scale in Fig. 10. After a short transient period in which all other modes but the high-Q mode radiate away the energy in the defect mode undergoes a slow exponential decay. This quality factor exceeds 13,000.

Finally, as in the case of the TE modes, we find that the coupling to the continuum still is an important factor for determining the strongest localization in TE modes. Strongest localization does not always occur in structures with the largest guided-mode gap. Of course, a large gap does strengthen confinement along the waveguide in general; however, the midcap frequency should also be as low as possible, to reduce the overlap with the continuum of radiating modes.

4. CONCLUSION

In summary, our calculations demonstrate the possibility of achieving strong confinement of light at defects in periodic dielectric waveguides, even without the assistance of a complete photonic band gap. These resonances can have a high quality factor Q and might prove useful in various device designs, such as for microlaser cavities or filters. We have also been able to identify the features that are important for strong confinement for each of the two polarizations.

These results appear quite promising and suggest that similar effects may be operational in more realistic 3-D rib-waveguide-cavity geometries. The properties of spontaneous emission in such cavities and their effect on lasing are also important problems that will need to be addressed in the future.

ACKNOWLEDGMENTS

The authors thank P. R. Villeneuve for many helpful discussions. This study was supported in part by the U.S. Army Research Office, contract DAAH04-93-G-0262, and the National Science Foundation/Materials Research Laboratory, contract DMR 90-22933.

REFERENCES

1. For a review, see the feature issue on the development and applications of materials exhibiting photon band gaps, J. Opt. Soc. Am. B **10,** 280–413 (1993).
2. R. D. Meade, K. D. Brommer, A. M. Rappe, and J. D. Joannopoulos, Phys. Rev. B **44,** 13,772 (1991).
3. H. A. Haus and C. V. Shank, IEEE J. Quantum Electron. **QE-12,** 532 (1976).
4. J. N. Winn, R. D. Meade, and J. D. Joannopoulos, J. Mod. Opt. **41,** 257 (1994).
5. R. D. Meade, A. M. Rappe, K. D. Brommer, J. D. Joannopoulos, and O. L. Alerhand, Phys. Rev. B **48,** 8434 (1993).
6. J. N. Winn, "Dynamic studies of photonic crystals," M.S. thesis (Massachusetts Institute of Technology, Cambridge, Mass., 1994).
7. B. Engquist and A. Majda, Math. Computat. **31,** 629 (1977).
8. A. Taflove and K. R. Umashankar, J. Electromagn. Waves Appl. **1,** 243 (1987).
9. A. Yariv, *Optical Electronics* (Saunders, Philadelphia, 1991).
10. R. D. Meade, A. M. Rappe, K. D. Brommer, and J. D. Joannopoulos, J. Opt. Soc. Am. B **10,** 328 (1993).